Journal of Quantitative Spectroscopy & Radiative Transfer 297 (2023) 108486

Contents lists available at ScienceDirect

Journal of Quantitative Spectroscopy & Radiative Transfer

journal homepage: www.elsevier.com/locate/jqsrt

Radiative transition probabilities of neutral and singly ionized rare earth elements (La, Ce, Pr, Nd, Sm, Gd, Tb, Dy, Ho, Er, Tm, Yb, Lu) estimated by laser-induced breakdown spectroscopy

Sawyer Irvine[a,b], Hunter Andrews[a,*], Kristian Myhre[a], Jamie Coble[b]

[a] Oak Ridge National Laboratory, 1 Bethel Valley Rd., Oak Ridge, TN 37830, USA
[b] University of Tennessee, Knoxville, TN 37996, USA

ARTICLE INFO

Article history:
Received 28 September 2022
Revised 21 December 2022
Accepted 6 January 2023
Available online 9 January 2023

Keywords:
REEs
Laser-induced breakdown spectroscopy (LIBS)
laser-ablation
Einstein coefficient
Saha-Boltzmann

ABSTRACT

Rare earth elements (REEs) are essential to society given their prevalence in many modern technologies. Quantitative elemental analysis of REEs is therefore a critical capability. Calibration free–laser-induced breakdown spectroscopy (CF-LIBS) is a rapidly maturing and promising approach to quantitative elemental analysis with many attractive qualities. The application of CF-LIBS to analyzing samples containing the REEs is hindered by a lack of fundamental data, specifically transition probabilities (TPs). This study seeks to help address this knowledge deficiency by reporting 967 previously unreported TPs for 13 REEs (lanthanum, cerium, praseodymium, neodymium, samarium, gadolinium, terbium, dysprosium, holmium, erbium, thulium, ytterbium, and lutetium). The method developed in this study to estimate the TPs requires small amounts of material (a few nanograms) compared with other approaches (∼ milligrams), uses non-specialized equipment, and does not involve complicated sample preparations.

1. Introduction

The rare earth elements (REEs) are ubiquitous with modern science and technology because of their unique chemical and nuclear properties. REEs elements are key components of magnetic, optical, anticorrosion, and other advanced materials used in everyday technologies. Certain isotopes of the REEs have attractive nuclear properties for use in radioisotope production targets, diagnostic and therapeutic agents in the field of nuclear medicine, as well as in quantum materials used in quantum information science [1–3]. The presence and concentration of several REEs in stellar media is also of high interest for extending human understanding of the universe. Yet, experimentally determined transition probabilities (TPs) for many electronic transitions in neutral and ionized atomic REE species remain unreported in the literature. However, there are databases which supplement these experimental values with values determined by ab-initio methods, such as the Kurucz database [4]. Additional experimental data would be helpful in the areas of both basic and applied science and technology. Of particular interest to our group is the use of TPs in calibration free–laser-induced breakdown spectroscopy (CF-LIBS).

Laser-induced breakdown spectroscopy (LIBS) can be used to quantify nearly every element in the periodic table, including low and high Z elements, stable and radioactive species, and samples of any physical form (e.g., solids, liquids, gasses, and aerosols). Recently, LIBS has been used to detect REEs in graphite matrices in ranges as low as 30 ppm [5,6], monitor them in aerosol streams in real-time [7], and to map them in glass-ceramic nuclear waste [8].

LIBS involves firing a focused laser pulse such that the power density (irradiance) at the sample surface is enough to ablate the material and form a plasma. As the generated plasma cools, energy is released as optical light with emissions characteristic of the elemental makeup of the sample. LIBS signals are not based on mass like mass spectrometry. This circumvents isobaric interferences that can be commonly encountered with REE mass spectrometry. Instead, a primary challenge faced by REE LIBS is the complexity of REEs emissions having many overlapping lines. Despite this, REE LIBS emission profiles offer many peaks to analyze, providing avenues to model these complex systems. Another advantage of LIBS is that it can be employed remotely through optical fibers, periscope systems, or at large distances through telescope systems so that samples can be analyzed within hazardous environments [9–22]. The caveat to the traditional LIBS approach is that it requires matrix-matched standards to construct a calibration curve before analyzing unknown samples. This generally requires a significant amount of material (∼grams), which is very limited for rare materials.

* Corresponding author.
E-mail address: andrewshb@ornl.gov (H. Andrews).

https://doi.org/10.1016/j.jqsrt.2023.108486
0022-4073/

CF-LIBS, originally proposed by Ciucci et al., could enable more time conservation, material conservation, and lessen exposure time [23]. CF-LIBS relies on the assumption that the plasma is under local thermodynamic equilibrium (LTE) during the time of data acquisition, which has been shown to be accurate under CF-LIBS applied situations [24–27]. When under LTE conditions, the electron density is high enough that the collisional rates exceed the radiative rates, the concentration calculations can be dependent on previously known fundamental values such as TPs. Leveraging the calibration on these previously reported values enables the foregoing of calibration curves made with matrix-matched samples. This saves time, reduces the resources necessary for measurement, and keeps exposure to a minimum. CF-LIBS can be completed by ablating a sample, collecting the spectra, and performing Saha-Boltzmann analysis to quantify the sample composition. As previously stated, this is dependent on the fundamental values being reported.

The primary barrier for use of CF-LIBS to quantitatively analyze for the REEs is the absence of reported TPs for many transitions of neutral, singly, and doubly ionized atomic species under LIBS plasma relevant conditions. Another issue is that the typical methods for estimating these values are material intensive, such as laser-induced fluorescence using a sputtered source from a hollow cathode tube [28–30]. Other methods such as Dirac Hartree-Fock, relativistic configuration interaction methods, and LIBS techniques have been used to produce TPs for praseodymium through gadolinium and copper [31,32]. This study proposes a method to use LIBS techniques with Saha-Boltzmann relations to calculate TPs. Similar methods were used in our previous studies on europium and neptuniuim [27,33]. This approach produces a large amount of data and suggests that it could be used for resource-restricted materials – such as the actinides – to enable further applications of CF-LIBS. The work presented here improves upon our previous studies by employing self-absorption corrections during data analysis to reduced associated uncertainties and expands the measurements to 13 additional REEs.

2. Experimental

2.1. Sample preparation

Thirteen REEs were examined during this study. These were lanthanum, cerium, praseodymium, neodymium, samarium, gadolinium, terbium, dysprosium, holmium, erbium, thulium, ytterbium, and lutetium. An individual sample was prepared for each REE. Each REE sample was spiked with strontium as an internal standard. Strontium was selected because of its strong spectral response and emission peaks with well-known, low-uncertainty TPs. Strontium boasts similar benefits as helium which is used as the typical standard in discharge lamps; however, it can be directly mixed into the sample solution whereas helium could not. This avoids any effects from inhomogeneous distribution of elements within the plasma. Each REE and strontium mixture was made from Inorganic Ventures 10,000 μg ml^{-1} inductively coupled plasma standards. Three different molar ratios were 10, 5, and 2 were prepared for each REE/strontium combination. A 10 µl droplet of each solution was pipetted onto individual aluminum-6061 pucks. The aluminum pucks were machined to have a small recession in the center where the droplet would rest. The pucks were placed onto a hot plate and set to a low temperature until the solution had completely dried. Duplicate samples were prepared for each concentration, as well as two strontium-only samples. Both the varied molar ratios and the use of duplicate samples were adjustments made from previous studies intended to help increase confidence in the TPs determined in this study [27,33].

2.2. Laser-Induced breakdown spectroscopy measurements

All LIBS measurements were performed using the same laser system detailed previously [27,33,34]. Briefly, the system included an Applied Photonics LIBSCAN 150 system using a fundamental wavelength of 1064 nm, a pulse energy of 161 ± 2.25 mJ, a pulse length of 5 ns, a spot size diameter of 500 µm, a laser fluence of 82 J cm^{-2}, and a Catalina Scientific Instruments EMU-120/65 echelle spectrometer. Collected spectra were measured with a gate delay of 1 µs and a gate width of 100 µs. Before any measurements were taken, the spectrometer wavelength was calibrated using a StellarNet, Inc., SL2 mercury argon lamp, and the spectral efficiency was calculated using a StellarNet, Inc., SL1-CAL tungsten halogen lamp with a certified spectrum.

Blank aluminum pucks were used to optimize the arrangement settings of the translation stage. Each test sample was placed in the LIBS unit on the translation stage and shot in a star pattern in 9 different spots, 5 times at each spot, providing 45 spectra per sample. Every 15 sequential spectra (3 spots) were averaged prior to analysis.

2.3. Spectra processing

The analyzed spectra were corrected using a determined relative efficiency function based on the optical arrangement of the system. This included the collection lenses, optical fiber, and the spectrometer itself. The relative efficiency function was determined by relating the average of 10 measured spectra of a calibration lamp to its certified spectrum. Additional information about the procedure can be found in our previous work [27,33]. After the efficiency correction was completed, the spectra were background corrected. The background correction was performed based off of the work done by Yaroshchyk and is detailed elsewhere [27,35].

Lastly, each spectrum was normalized to the 396.15 nm Al I peak intensity. Normalizing the spectra aided in correcting for shot-to-shot laser energy variation. This shot-to-shot variation alters the amount of energy distributed into the sample, which then impacts the amount of material ablated and the formation of the plasma. Both normalizing and averaging mitigate this variance. This Al peak in several different REE spectra is shown overlaid in Fig. S1. An alternative normalization approach would be to fit the Al peak and normalize to the peak's area which may account for ablation differences slightly differently by considering the peak width change; however, as seen in Fig. S1 there is little change in the peak shape indicating intensity normalization was sufficient.

2.4. Peak identification and fitting

The neutral and singly ionized energy levels of each REE, taken from the Basic Atomic Spectroscopic Database hosted by the National Institute for Standards and Technology, were used to calculate all possible transitions that would result in emissions in the visible spectrum. For each REE these calculated emission wavelengths were compared to preprocessed spectra of a blank aluminum sample, a sample with only strontium, and a sample with a REE and no strontium. The spectra were then meticulously scanned to identify REE species' peaks available for further analysis.

After all of the available peaks were identified, the lmfit package in Python was used to fit Voigt functions to the emission peaks [36]. Voigt functions are a convolution of Lorentzian and Gaussian functions; this combination is typically used for fitting LIBS peaks [26]. The widths of the Lorentz and Gaussian component of the Voigt profile changes from peak to peak and sample to sample, which is why each peak must be fit individually. The peak centers and areas were then determined using the Voigt fits and used in further analysis as the integral intensity. Peaks were matched

with transition information based on their Voigt fit centers; it is important to note there is some uncertainty here.

2.5. Saha-Boltzmann analysis

The integral intensity I_{nm} of an electronic transition of species s from energy level n to m can be calculated as a function of several parameters. The Saha equation, another vital descriptor of the emissions of an LTE plasma, describes the ratio between the concentrations of species at different ionization levels [27,37,38]. The equations for the integral intensity and Saha relationship, respectively, are as follows:

$$I_{nm} = F(\lambda)C_s\frac{A_{nm}g_n}{U_s}\exp\left(\frac{-E_n}{T}\right), \tag{1}$$

where I is the integral intensity, $F(\lambda)$ is the instrument function (efficiency), C_s is the number density of species s, A is the TP, g is the level degeneracy, E is the ionization energy, T is plasma temperature, and U_s is the partition function of species s at a given plasma temperature.

$$\frac{C_2}{C_1} = \frac{(2\pi m_e T)^{3/2}}{n_e h^3}\frac{2U_2}{U_1}\exp\left(\frac{-E_{ion}}{T}\right), \tag{2}$$

where 1 and 2 refer to separate upper and lower ionization states, respectively, m_e is the electron mass, n_e is the electron density, h is Plank's constant, and E_{ion} is the ionization energy [37,38]. As detailed in our previous work, combining the integral intensity and Saha equations Eqs. (3) and (4) provides the Saha-Boltzmann relation, which can be written in a linear form as

$$y = mx + b(T) \ where \begin{cases} m = -\frac{1}{T}, \ b(T) = ln\left(\frac{FC_1}{(U_1)}\right), \\ x = \begin{cases} E_1 \ (neutral), \\ E_2 + E_{ion} \ (ionic), \end{cases} \\ y = \begin{cases} ln\left(\frac{I_1}{g_1A_1}\right) \ (neutral), \\ ln\left(\frac{I_2}{g_2A_2}\right) - ln\left(\frac{2(2\pi m_e T)^{\frac{3}{2}}}{h^3 n_e}\right) (ionic) \end{cases} \end{cases} \tag{3}$$

The electron density and plasma temperature are needed for the Saha-Boltzmann method. The electron density was obtained using Eq. (4), which relates the Stark broadening associated with the Balmer series hydrogen alpha line, which was strongly visible in our spectrum, and its full width half max ($\Delta\lambda$) from de Oliveira Borges [39]. The electron density was calculated for each sample spectrum. An improvement to be made in future studies would be to account for the spectrometer's instrument broadening prior to this calculation.

$$n_e = \left[\left(\frac{\Delta\lambda}{0.549}\right)^{1.4713}\right]10^{17} . \tag{4}$$

The temperature was calculated through iteratively fitting the Saha-Boltzmann graphs (Eq. (3)). An initial temperature guess was provided to a Python script, then Saha-Boltzmann coordinates were calculated, and a line was fitted. A new temperature was determined from the slope of this fitted line. This process was looped until the percent difference of the temperature from the previous iteration and the current iteration was below 0.0001%. This was done for both the strontium and the REE of each sample. It was observed that the strontium temperature was slightly different than each of the REE temperatures and that the REE temperatures had more spread in their data. The reader is referred elsewhere for more information on this method for determining the plasma temperature [40].

Given that the spectra were efficiency corrected and repeatable, this spread about the Saha-Boltzmann fit was attributed to self-absorption, a common occurrence in LIBS spectra. The preferred method of self-absorption correction is to use Stark broadening coefficients when available. This was possible for the two ionized strontium peaks used in this study, both of which showed characteristics of self-absorption. The remaining emissions were corrected using the Internal Reference for Self-Absorption Correction (IRSAC) methodology developed by Sun and Yu [41]. The IRSAC method was performed as follows. The transitions that are affected the most by self-absorption are often ones with large TPs and low upper energy levels. Based on this logic, the neutral and ionized transitions were ranked to identify the emissions with the lowest TPs and highest upper energy levels. Each trait was weighed equally to form an overall rank, and the neutral and singly ionized peaks with the highest overall ranks were chosen to be the self-absorption reference peaks. The remaining emission peaks were then adjusted using the self-absorption coefficients calculated as

$$f_\lambda^b = \frac{I_\lambda^{ij}A_{mn}g_m}{I_{\lambda R}^{mn}A_{ij}g_i}e^{\frac{-E_m+E_i}{T}}, \tag{5}$$

where R indicates the reference peak, m/n refer to the upper and lower states of the reference line, and i/j refer to the upper and lower states of the line being corrected. The initial temperature used was from the Saha-Boltzmann iterative fitting previously discussed. Once the f-value for each peak was calculated, the intensities of the non-reference peaks were divided by the f-values to provide adjusted integral intensities. Although the reference peaks are assumed to have no self-absorption, there is a possibility of minor levels. If a peak had an f-value greater than 1 that indicated it was experiencing less self-absorption than the reference peaks. When this occurred, the f-value was set to 1 so that the intensity would not be altered. The IRSAC method uses an iterative procedure where the emission peaks were corrected, and a new Saha-Boltzmann plot was calculated. The new Saha-Boltzmann coordinates were then used to correct the emissions again. The process was iterated through until the coefficient of determination (R^2) differences between iterations were less than 0.01%.

3. Results and discussion

A total of 78 samples were tested in this study to estimate new TPs for 13 REEs. The remaining two REEs not studied are europium and promethium. Europium was measured in a previous study [27]. Promethium is the only REE without a stable isotope, making the element not only rare but also requiring proper radiological controls which were otherwise unneeded in this study. Each REE spectrum was parsed to match emission peaks with energy level transitions. The spectra of the REE samples, along with the Al and Sr spectra, are shown in Fig. 1. Zoomed spectra plots for Ce, Dy, Er, and Pr are shown in the Fig. S2 of the Supporting Information. Even when visualizing 100 nm of wavelength, differences between all the spectral signatures of each REE can be seen.

The emission lines observed in this study ranged between 350 and 650 nm. The lower end of this range was the result of the optical efficiency, which was significantly reduced below 350 nm. Lines for oxygen and nitrogen were very prevalent above 650 nm and overwhelmed most of the spectra beyond that point. The REE peaks that were found in this study were primarily ionized peaks, although many neutral peaks were found as well. This behavior is seen in many other studies, as the ionized peaks tend to have greater emission intensities than the neutral peaks [42–46]. Fig. 2 shows the theoretical comparison of neutral versus singly ionized theoretical emission and normalized intensities for lanthanum, cerium, and neodymium. In Fig. 2(a), the ionized emissions are shown to be much more intense than neutral emissions. In Fig. 2(b), both neutral and singly ionized peaks are shown to be in balance with one another for the temperatures seen in this

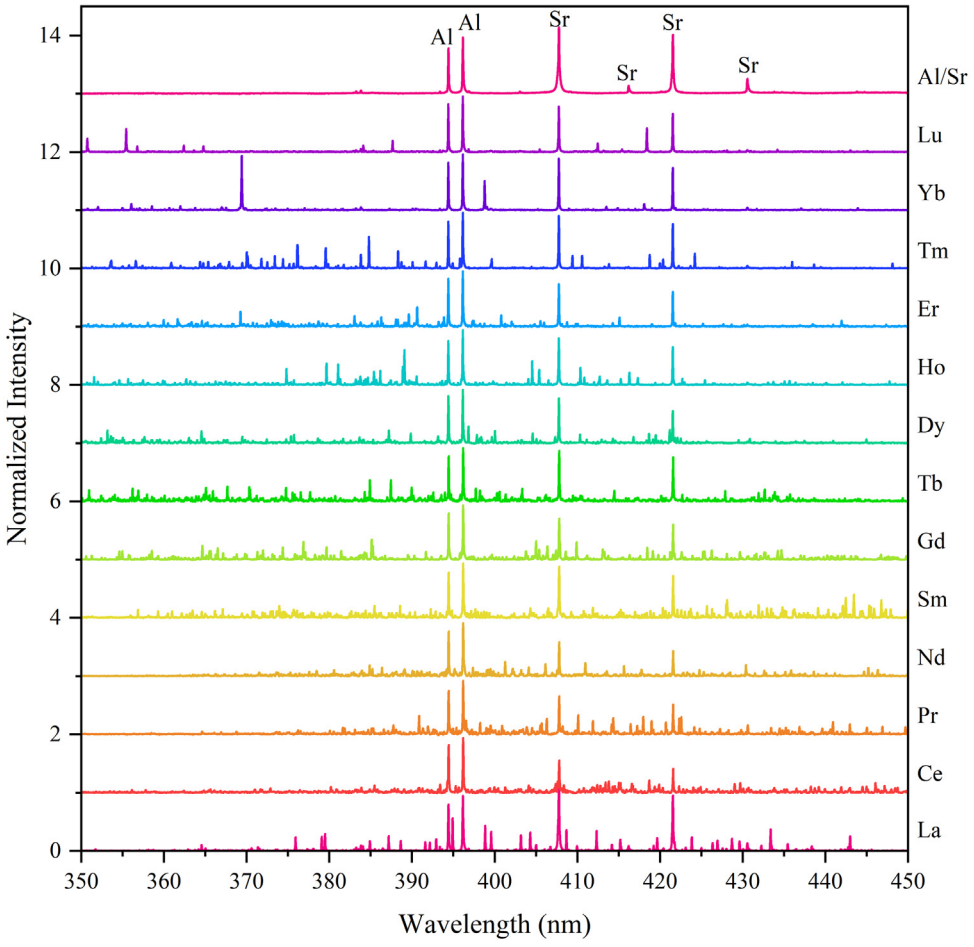

Fig. 1. Stacked comparison of REE spectra to the spectrum of the Al substrate and Sr standard blank illustrating the number of peaks available for analysis in this study.

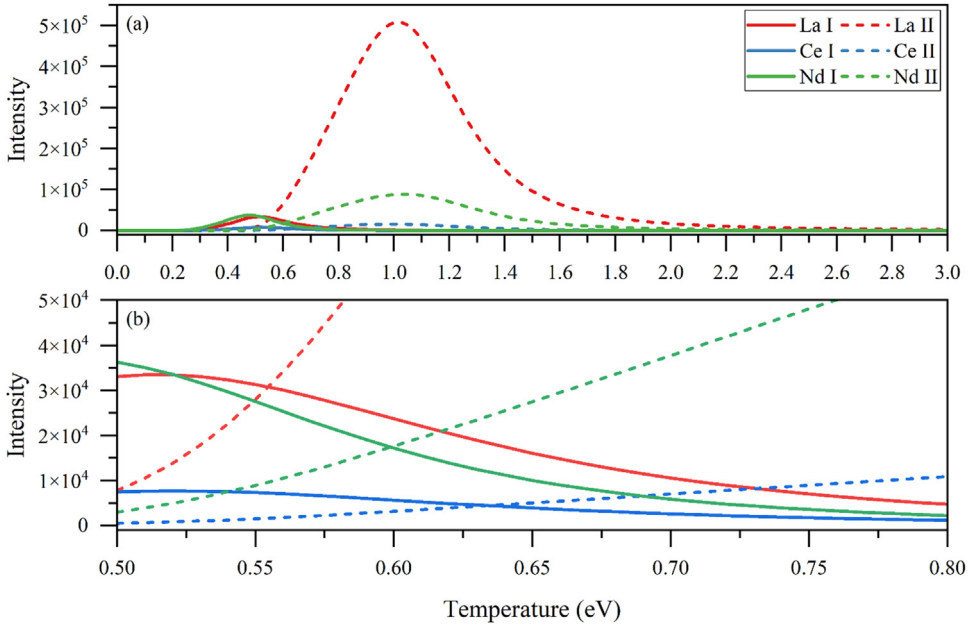

Fig. 2. Comparison of neutral versus singly ionized (a) theoretical emission intensities and (b) zoomed in temperature region showing the crossover between neutral and singly ionized populations.

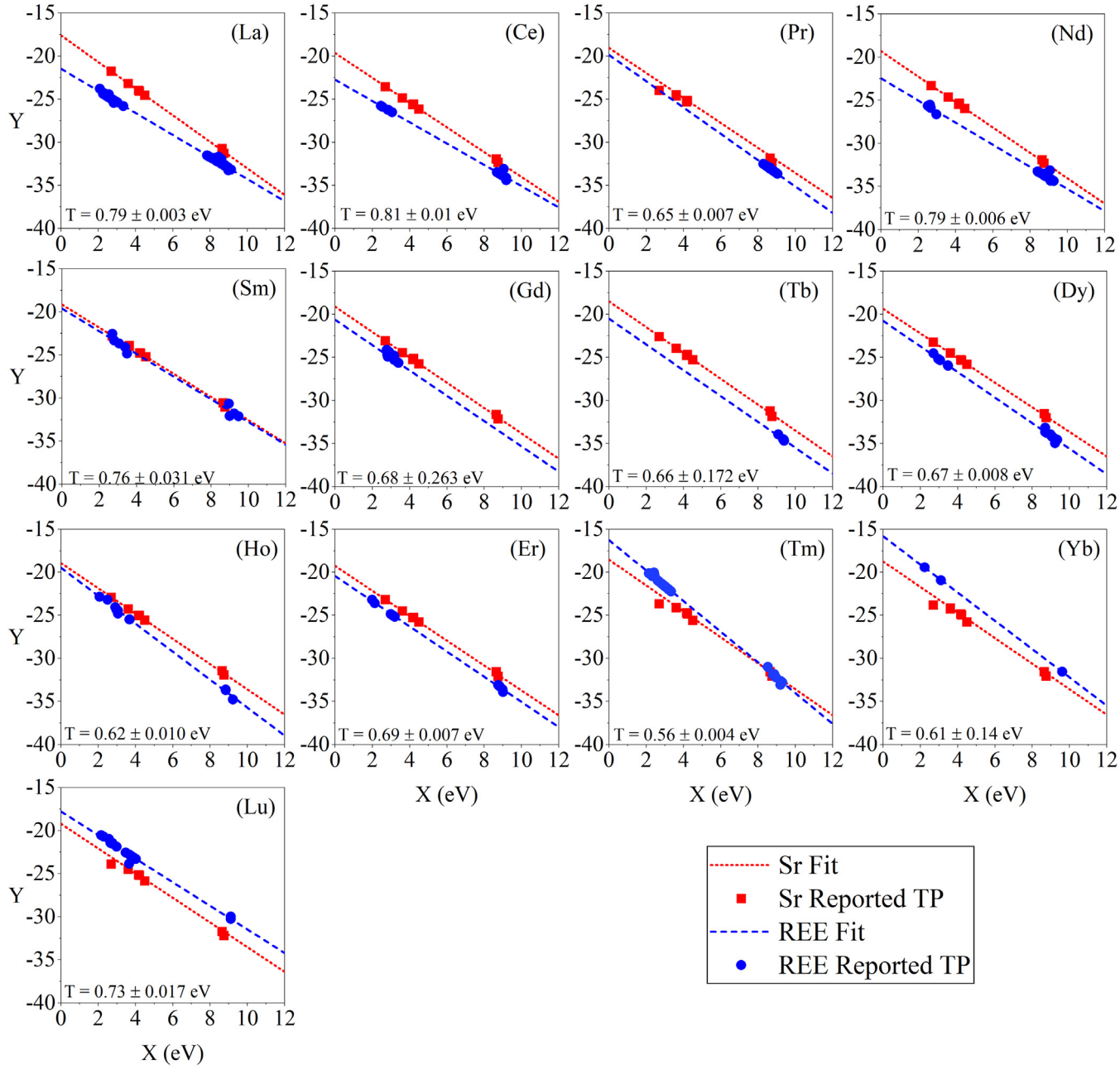

Fig. 3. Saha-Boltzmann plots for each REE after self-absorption correction. The shown plots are for the 10:1 REE:strontium molar ratio samples.

study (e.g., 0.6–0.8 eV). However, because neutral peaks are much lower in their maximum intensity than ionized peaks, they are much more susceptible to being lost in the background emissions. Future work could intentionally test samples at different laser energies and delay times to measure the plasma at different temperatures to target different ionization states.

The fitted peak areas were used to construct Saha-Boltzmann plots, which were then adjusted for self-correction using the IRSAC procedure. These plots are shown in Fig. 3 for each element. There is a trend among the Saha-Boltzmann plots where the REE lines slowly rise above the strontium lines as the elemental mass increases; the slopes remain similar, but the intercept slowly increases across the series. Each temperature reported is the REE temperature. For gadolinium and terbium, their slopes were forced to match the strontium slope, as disclosed subsequently, and the temperature is still within good agreement with the other temperatures in this study.

The strontium and REE slopes (temperature) were commonly within 90% of one another in most samples, as is expected under LTE assumptions. Although the strontium and REE slopes were typically solved independently of one another, there were exceptions in cases where limited reported TPs were available. For the gadolinium and terbium samples, the plasma temperature was calculated from the strontium slope and the intercept was determined using the limited lines with reported TPs. This was done based on the assumption that the plasma temperature is homogonous during LTE. Samarium was lacking TPs for the neutral state; however, the slope estimated with the ionized values produced a temperature that agreed well with the strontium temperature, so the samarium slope was not forced to match strontium.

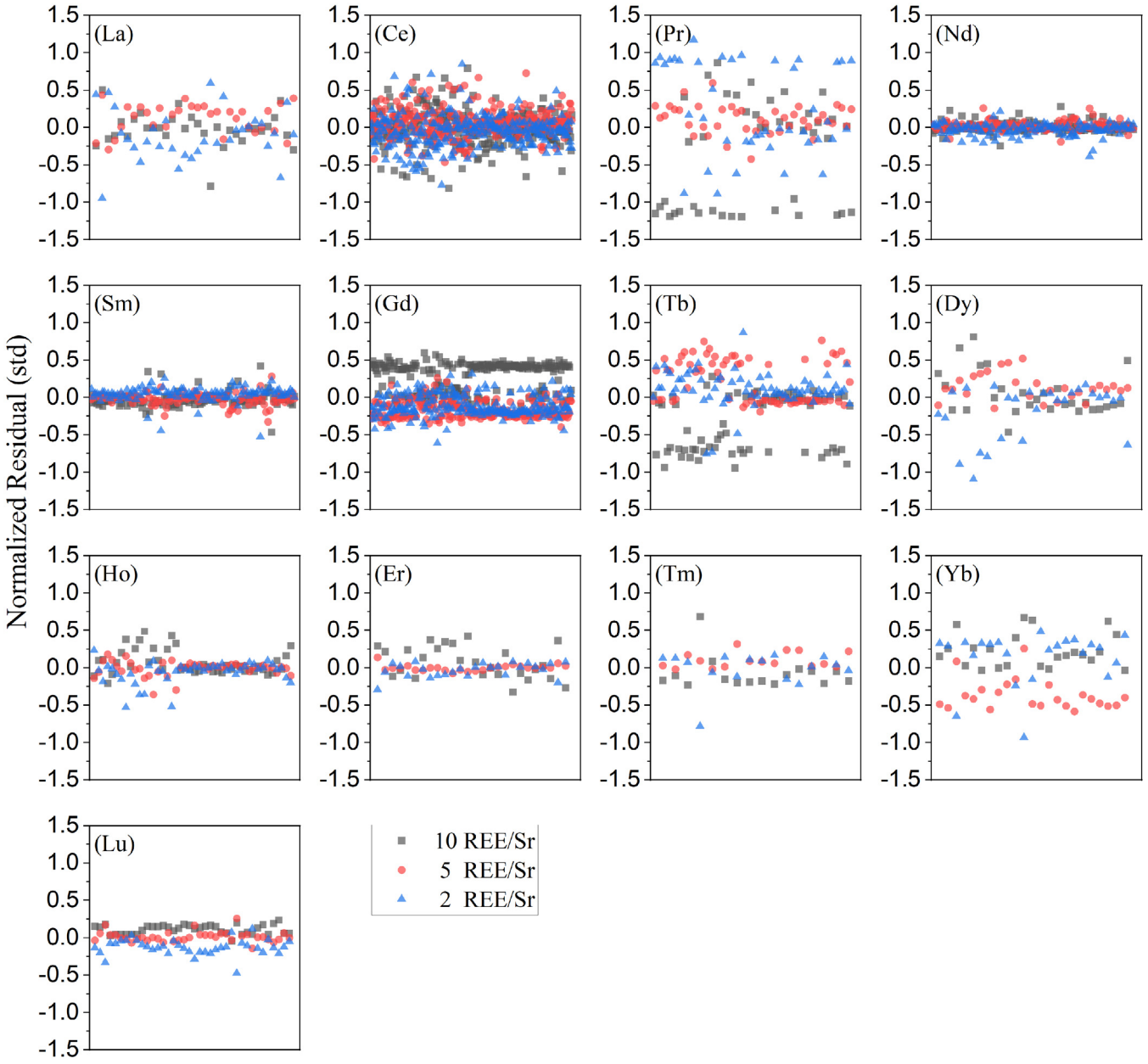

Fig. 4. Estimated TPs residuals compared to the mean values reported in the Supporting Information. The vertical axis is in terms of standard deviation from the mean, where zero represents a strong match.

The final Saha-Boltzmann plot fits were used to estimate new TPs and their associated uncertainties. The TPs and uncertainties from the multiple samples of each REE were combined to get a final value for each emission peak. The tabulation of all TPs estimated in this study are reported in Tables S.7–S.17 in elemental order, along with ionization levels, energy levels, and degeneracies.

A comparison calculated TP residuals from the Gaussian-averaged values is shown in Fig. 4 (note the vertical axis is in terms of standard deviation). The residuals show that all sample calculations fall within 1.5 standard deviations of the Gaussian average, most being closer. According to Fig. 4, praseodymium, gadolinium, and terbium showed the largest deviations. These three REEs had only neutral or only ionized values previously reported meaning that their Saha-Boltzmann plots required a greater reliance on strontium as the internal standard and more prone to errors from an unequal distribution of previously reported values. Also note that for gadolinium and terbium the 10 REE/strontium ratio sample had the largest standard deviation. Strontium has the lowest concentration in these samples, and it is possible that this led to a higher error when forcing temperatures of the REE to match that of the strontium. Even though these samples had higher standard deviation this did not result in a higher Gaussian uncertainty than the other samples, even praseodymium had uncertainty down to 12%. Again, this was possible due to the large amount of data that was able to be collected, which resulted in lowering the uncertainties.

TPs calculated in this study are compared with literature values in Tables S.1–S.6 and are shown in Fig. 5. Limited values were available for comparison for the REEs; there were no comparison values found for Dy, Ho, Er, Tm, Yb, and Lu. Many of these heavier REEs had reported values for transitions not applicable for LIBS (e.g., higher ionization states (ion > III) or diatomic molecular transitions). LIBS typically produces plasmas containing neutral and singly ionized species. Additionally, only exact wavelength matches

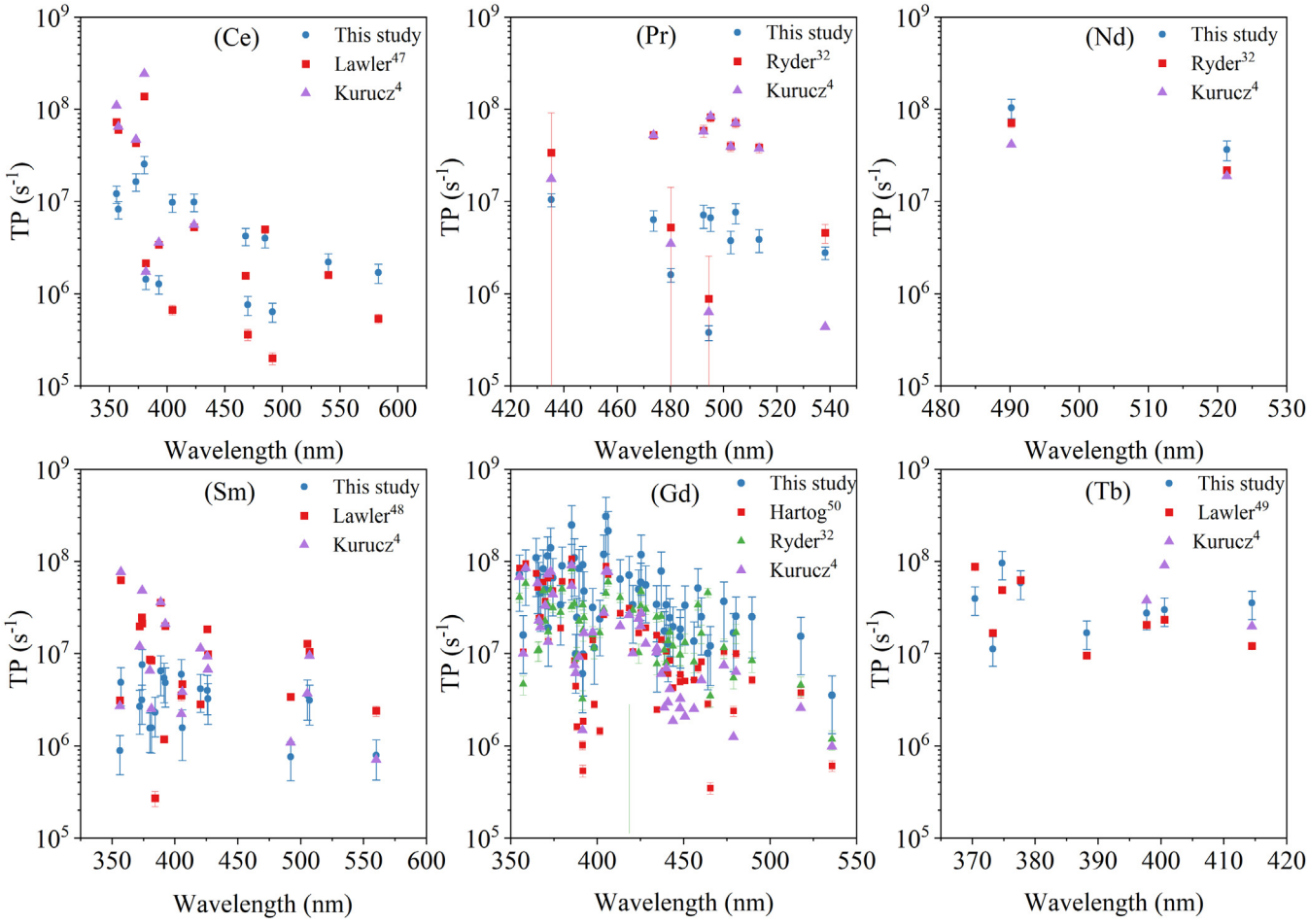

Fig. 5. TPs calculated in this study (blue) compared with other studies (red, green, purple) [4,32,47–50].

are shown. Many of the transitions reported by Lawler et al. were not matched in this study; this is likely due to many weak emissions being discarded in this study as not having a significant magnitude to carry through further analysis [47]. The Kurucz database was also parsed for matches.

Previous TPs studies done by Den Hartog and Lawler used laser-induced fluorescence and Fourier transform spectroscopy for europium, gadolinium, holmium, and cerium. Rehse and Ryder used a similar LIBS setup (1064 nm Nd-YAG, Echelle spectrometer) to measure branching fractions and then calculate TPs and other fundamental data for neodymium, samarium, gadolinium, and gallium [32,51]. Most of the shown values from the Kurucz database come from modeling [4]. Multiple stages of agreement exist among the values estimated in this study and those reported in literature. For cerium, most of the TPs differ but appear to follow similar trends over the set. In the praseodymium comparison, three of the reference values have larger errors that overlap with our values. Most of the reference values are above our values. The neodymium TPs show good agreement. The samarium TPs seem to be mixed; while there is some overlap, most of the reference values are above those calculated in this study. Gadolinium shows good agreement and provides insight into the level of spread between multiple studies. Lastly, the terbium TPs show agreement as they rest close to or overlap with the reference values. The values from the Kurucz database show a similar range of agreement across the REEs shown. The Kurucz values appear to show strong agreement with the values from Ryder, but Ryder reported the database and their calculated values differed with average percent differences ranging from −47–74.1%.

Several of the emission peaks with new TPs estimated in this study have been used in previous studies for tradition LIBS (i.e., to build calibration curves). Martin et al. investigated several REEs at low concentrations (30–300 ppm) to identify lines that could be used for quantification at that level. Out of the peaks tabulated by Martin et al., this study determined new TPs for the 358.496, 364.619, 374.347, and 418.425 nm gadolinium II peaks [5]. In a previous study by our group, Andrews and Myhre developed a LIBS system to monitor the off-gas stream from a molten salt reactor, a type of advance nuclear reactor, in real- time [7]. Many REEs are common by-products of nuclear fission, making them of interest for monitoring. In said study, three lanthanides were investigated including gadolinium, neodymium, and samarium in an aerosol stream [7]. Transitions probabilities were estimated for several of the peaks listed: the 404.986, 418.425, and 425.173 nm gadolinium II peaks and the 442.434 nm samarium II peak [7]. Campbell et al. report a list of strong Ce emissions that were used for quantification of Ce in simulated nuclear fuel. Many of these peaks are at similar wavelengths to those reported in this study, but slight discrepancies are likely related to the apparent peak center reported by Campbell to the Voigt centers reported here [52]. These studies exemplify how the newly estimated TPs from this study would enable the application of CF-LIBS for ranging from quantifying REEs for critical material recovery to monitoring the proper treatment hazardous waste streams.

4. Conclusion

In this study, 967 new TPs were estimated using LIBS spectra, Saha-Boltzmann methods, and self-absorption correction. The fundamental parameters reported in this study may contribute to the astrophysics community so that spectra collected from stellar objects can be interpreted more thoroughly. More importantly, this study has shown that LIBS methods can be used to estimate new TPs with high-throughput and with uncertainties as low as 10%. It was found in this study that neutral peaks typically result in lower uncertainty than ionized peaks, which is likely due to ionized peaks having much greater intensities that are subject to more self-absorption. Depending on the number of replicates measured and the ability to collect repeatable and well-behaved (low self-absorption present) data from the spectra, it is possible to significantly reduce uncertainty, as seen when comparing this study's uncertainty levels to our previous europium study [27].

This study has confirmed that increasing the number of samples allows the uncertainty in the TPs to be reduced. Even though the number of samples was increased in this study, the amount of analyte used was still very low (milligrams). Using reported energy levels to calculate all possible transitions guided peak identification and enabled more data to be used for calculating Saha-Boltzmann plots, and thereby estimate more TPs. The authors suggest that this method be considered in future studies, especially with the rare materials, to maximize the amount of data one can produce with reduced uncertainty. Future work would see the methods from this study applied to promethium and the actinide series elements, further expanding the applicability of CF-LIBS. Additionally, tailoring gating times and laser energies may provide additional transitions to be evaluated and the inclusion of additional model constraints such as branching ratios may result in more accurate TPs.

Declaration of Competing Interest

The authors declare that they have no known competing financial interests or personal relationships that could have appeared to influence the work reported in this paper.

CRediT authorship contribution statement

Sawyer Irvine: Methodology, Investigation, Software, Writing – original draft, Writing – review & editing, Visualization. **Hunter Andrews:** Conceptualization, Methodology, Investigation, Software, Writing – original draft, Writing – review & editing, Visualization, Funding acquisition, Project administration. **Kristian Myhre:** Conceptualization, Methodology, Writing – review & editing. **Jamie Coble:** Methodology, Writing – review & editing.

Data availability

The data underlying this article will be shared on reasonable request to the corresponding author.

Acknowledgments

This research was supported by the US Department of Energy Isotope Program, managed by the Office of Science for Isotope R&D and Production.

Supplementary materials

Supplementary material associated with this article can be found, in the online version, at doi:10.1016/j.jqsrt.2023.108486.

References

[1] Wallerstein G, Iben I, Parker P, Boesgaard AM, Hale GM, Champagne AE, Barnes CA, Käppeler F, Smith VV, Hoffman RD, Timmes FX, Sneden C, Boyd RN, Meyer BS, Lambert DL. Synthesis of the Elements in Stars: Forty Years of Progress. Rev. Mod. Phys. 1997;69(4):995–1084. doi:10.1103/RevModPhys.69.995.

[2] Boll RA, Van Cleve SM, Sims NJ, Felker LK, Burns JD, Owen GD, Smith EH, White CS, Ezold JG. Californium Electrodepositions at Oak Ridge National Laboratory. J. Radioanal. Nucl. Chem. 2015;305(3):921–6. doi:10.1007/s10967-015-4148-8.

[3] Knapp Ff Jr., Mirzadeh S, Beets Al, Du M. Production of Therapeutic Radioisotopes in the ORNL High Flux Isotope Reactor (HFIR) for Applications in Nuclear Medicine, Oncologyand Interventional Cardiology. J. Radioanal. Nucl. Chem. 2005;263(2):503–9. doi:10.1007/s10967-005-0083-4.

[4] *Atomic spectral line database from CD-ROM 23 of R. L. Kurucz*. https://lweb.cfa.harvard.edu/amp/ampdata/kurucz23/sekur.html (accessed 2022-12-20).

[5] Martin M, Martin RC, Andrews HB, Allman S, Brice D, Martin S, Nicolas A. Quantification of Rare Earth Elements in the Parts Per Million Range_ A Novel Approach in the Application of Laser-Induced Breakdown Spectroscopy.Pdf. Appl. Spectrosc 2022;0:1–9. doi:10.1177/00037028221092051.

[6] Martin M, Martin RC, Allman S, Brice D, Wymore A, Andre N. Quantification of Rare Earth Elements Using Laser-Induced Breakdown Spectroscopy. Spectrochim. Acta Part B At. Spectrosc. 2015;114:65–73. doi:10.1016/j.sab.2015.10.005.

[7] Andrews HB, Myhre KG. Quantification of Lanthanides in a Molten Salt Reactor Surrogate Off-Gas Stream Using Laser-Induced Breakdown Spectroscopy. Appl. Spectrosc. 2022 00037028211070323. doi:10.1177/00037028211070323.

[8] Wang X, Motto-Ros V, Panczer G, De Ligny D, Yu J, Benoit JM, Dussossoy JL, Peuget S. Mapping of Rare Earth Elements in Nuclear Waste Glass–Ceramic Using Micro Laser-Induced Breakdown Spectroscopy. Spectrochim. Acta Part B At. Spectrosc. 2013;87:139–46. doi:10.1016/j.sab.2013.05.022.

[9] Guirado S, Fortes FJ, Lazic V, Laserna JJ. Chemical Analysis of Archeological Materials in Submarine Environments Using Laser-Induced Breakdown Spectroscopy. On-Site Trials in the Mediterranean Sea. Spectrochim. Acta Part B At. Spectrosc. 2012;74–75:137–43. doi:10.1016/j.sab.2012.06.032.

[10] Nakanishi R, Saeki M, Wakaida I, Ohba H. Detection of Gadolinium in Surrogate Nuclear Fuel Debris Using Fiber-Optic Laser-Induced Breakdown Spectroscopy under Gamma Irradiation. Appl. Sci. 2020;10(24):8985. doi:10.3390/app10248985.

[11] Saeki M, Iwanade A, Ito C, Wakaida I, Thornton B, Sakka T, Ohba H. Development of a Fiber-Coupled Laser-Induced Breakdown Spectroscopy Instrument for Analysis of Underwater Debris in a Nuclear Reactor Core. J. Nucl. Sci. Technol. 2014;51(7–8):930–8. doi:10.1080/00223131.2014.917996.

[12] Marquardt BJ, Goode SR, Angel SM. In Situ Determination of Lead in Paint by Laser-Induced Breakdown Spectroscopy Using a Fiber-Optic Probe. Anal. Chem. 1996;68(6):977–81. doi:10.1021/ac950828h.

[13] Sasazawa S, Kakino S, Matsuura Y. Optical-Fiber-Based Laser-Induced Breakdown Spectroscopy for Detection of Early Caries. J. Biomed. Opt. 2015;20(6):065002. doi:10.1117/1.JBO.20.6.065002.

[14] Rai AK, Zhang H, Yueh FY, Singh JP, Weisberg A. Parametric Study of a Fiber-Optic Laser-Induced Breakdown Spectroscopy Probe for Analysis of Aluminum Alloys. Spectrochim. Acta Part B At. Spectrosc. 2001;56(12):2371–83. doi:10.1016/S0584-8547(01)00299-3.

[15] Wu J, Qiu Y, Li X, Yu H, Zhang Z, Qiu A. Progress of Laser-Induced Breakdown Spectroscopy in Nuclear Industry Applications. J. Phys. Appl. Phys. 2020;53(2):023001. doi:10.1088/1361-6463/ab477a.

[16] Davies CM, Telle HH, Montgomery DJ, Corbett RE. Quantitative Analysis Using Remote Laser-Induced Breakdown Spectroscopy (LIBS). Spectrochim. Acta Part B At. Spectrosc. 1995;50(9):1059–75. doi:10.1016/0584-8547(95)01314-5.

[17] Cremers DA, Barefield JE, Koskelo AC. Remote Elemental Analysis by Laser-Induced Breakdown Spectroscopy Using a Fiber-Optic Cable. Appl. Spectrosc. 1995;49(6):857–60. doi:10.1366/0003702953964589.

[18] Whitehouse AI, Young J, Botheroyd IM, Lawson S, Evans CP, Wright J. Remote Material Analysis of Nuclear Power Station Steam Generator Tubes by Laser-Induced Breakdown Spectroscopy . At. Spectrosc. 2001:10.

[19] Fobar DG, Xiao X, Burger M, Le Berre S, Motta AT, Jovanovic I. Robotic Delivery of Laser-Induced Breakdown Spectroscopy for Sensitive Chlorine Measurement in Dry Cask Storage Systems. Prog. Nucl. Energy 2018;109:188–94. doi:10.1016/j.pnucene.2018.08.001.

[20] Beddows DCS, Samek O, Liška M, Telle HH. Single-Pulse Laser-Induced Breakdown Spectroscopy of Samples Submerged in Water Using a Single-Fibre Light Delivery System. Spectrochim. Acta Part B At. Spectrosc. 2002;57(9):1461–71. doi:10.1016/S0584-8547(02)00083-6.

[21] Fortes FJ, Laserna JJ. The Development of Fieldable Laser-Induced Breakdown Spectrometer: No Limits on the Horizon. Spectrochim. Acta Part B At. Spectrosc. 2010;65(12):975–90. doi:10.1016/j.sab.2010.11.009.

[22] Neuhauser RE, Panne U, Niessner R. Utilization of Fiber Optics for Remote Sensing by Laser-Induced Plasma Spectroscopy (LIPS). Appl. Spectrosc. 2000;54(6):923–7. doi:10.1366/0003702001950337.

[23] Ciucci A, Corsi M, Palleschi V, Rastelli S, Salvetti A, Tognoni E. New Procedure for Quantitative Elemental Analysis by Laser-Induced Plasma Spectroscopy. Appl. Spectrosc 1999;53(8):960–4. doi:10.1366/0003702991947612.

[24] Fu H, Ni Z, Wang H, Jia J, Dong F. Accuracy Improvement of Calibration-Free Laser-Induced Breakdown Spectroscopy. Plasma Sci. Technol. 2019;21(3):034001. doi:10.1088/2058-6272/aaead6.

[25] Tognoni E, Cristoforetti G, Legnaioli S, Palleschi V. Calibration-Free Laser-Induced Breakdown Spectroscopy: State of the Art. Spectrochim. Acta Part B At. Spectrosc. 2010;65(1):1–14. doi:10.1016/j.sab.2009.11.006.
[26] Aguilera JA, Aragón C. Characterization of a Laser-Induced Plasma by Spatially Resolved Spectroscopy of Neutral Atom and Ion Emissions. Spectrochim. Acta Part B At. Spectrosc. 2004;59(12):1861–76. doi:10.1016/j.sab.2004.08.003.
[27] Irvine S, Andrews H, Myhre K, Goldstein K, Coble J. Radiative Transition Probabilities of Neutral and Singly Ionized Europium Estimated by Laser-Induced Breakdown Spectroscopy. J. Quant. Spectrosc. Radiat. Transf. 2022:108184. doi:10.1016/j.jqsrt.2022.108184.
[28] Den Hartog EA, Wickliffe ME, Lawler JE. Radiative Lifetimes of Eu and Transition Probabilities of Eu. Astrophys. J. Suppl. Ser. 2002;141(1):255–65. doi:10.1086/340039.
[29] Zhiguo Z, Li ZS, Lundberg H, Zhang KY, Dai ZW, Zhankui J, Svanberg S. Radiative Properties of Eu II and Eu III Obtained from Lifetime and Branching Ratio Measurements. J. Phys. B At. Mol. Opt. Phys. 2000;33(3):521–6. doi:10.1088/0953-4075/33/3/319.
[30] Den Hartog EA, Wiese LM, Lawler JE. Radiative Lifetimes of HoI and HoII. J. Opt. Soc. Am. B 1999;16(12):2278. doi:10.1364/JOSAB.16.002278.
[31] Radžiūtė L, Gaigalas G, Kato D, Rynkun P, Tanaka M. Extended Calculations of Energy Levels and Transition Rates for Singly Ionized Lanthanide Elements. I. Pr–Gd. Astrophys. J. Suppl. Ser. 2020;248(1):17. doi:10.3847/1538-4365/ab8312.
[32] Ryder, C. Oscillator Strength Measurements in Singly-Ionized, Doubly-Ionized and Neutral Lanthanides and Transition Elements (Sm, Nd, Pr, Gd, Cu, and Fe) Using Laser-Induced Breakdown Spectroscopy. 2011, 555.
[33] Andrews HB, Sadergaski LR, Myhre KG. Neptunium Transition Probabilities Estimated through Laser Induced Breakdown Spectroscopy (LIBS) Measurements. J. Anal. At. Spectrom. 2022;37(4):768–74. doi:10.1039/D1JA00423A.
[34] Myhre KG, Mehta MJ, Martin MZ, Du M. Laser Induced Breakdown Spectroscopy Analysis of Europium and Samarium in Aluminum Oxide. Spectrochim. Acta Part B At. Spectrosc. 2018;149:30–4. doi:10.1016/j.sab.2018.07.014.
[35] Yaroshchyk P, Eberhardt JE. Automatic Correction of Continuum Background in Laser-Induced Breakdown Spectroscopy Using a Model-Free Algorithm. Spectrochim. Acta Part B At. Spectrosc. 2014;99:138–49. doi:10.1016/j.sab.2014.06.020.
[36] Newville, M.; Stensitzki, T.; Allen, D. B.; Ingargiola, A. LMFIT: Non-Linear Least-Square Minimization and Curve-Fitting for Python, 2014. https://doi.org/10.5281/zenodo.11813.
[37] Farooq Z, Ali R, Qurashi US, Mahmood MH, Yaseen M, Qayyum MA, Hussain MN, Shah SM, Jan T. Spectroscopic Studies of Laser Produced Plasma of Doped Nano-Structured Material by Laser Induced Breakdown Spectroscopy. Phys. Plasmas 2018;25(9):093106. doi:10.1063/1.5031828.
[38] Tognoni E, Cristoforetti G, Legnaioli S, Palleschi V. A Numerical Study of Expected Accuracy and Precision in Calibration-Free Laser-Induced Breakdown Spectroscopy in the Assumption of Ideal Analytical Plasma. Spectrochim. Acta Part B 2007;62:1287–302.
[39] de Oliveira Borges F, Ospina JU, de Holanda Cavalcanti G, Farias EE, Rocha AA, Ferreira PILB, Gomes GC, Mello A. CF-LIBS Analysis of Frozen Aqueous Solution Samples by Using a Standard Internal Reference and Correcting the Self-Absorption Effect. J. Anal. At. Spectrom. 2018;33(4):629–41. doi:10.1039/C7JA00299H.
[40] Zhang S, Wang X, He M, Jiang Y, Zhang B, Hang W, Huang B. Laser-Induced Plasma Temperature. Spectrochim. Acta Part B At. Spectrosc. 2014;97:13–33. doi:10.1016/j.sab.2014.04.009.
[41] Sun L, Yu H. Correction of Self-Absorption Effect in Calibration-Free Laser-Induced Breakdown Spectroscopy by an Internal Reference Method. Talanta 2009;79(2):388–95. doi:10.1016/j.talanta.2009.03.066.
[42] Andrews H, Phongikaroon S. Development of an Experimental Routine for Electrochemical and Laser-Induced Breakdown Spectroscopy Composition Measurements of $SmCl_3$ in LiCl-KCl Eutectic Salt Systems. Nucl. Technol. 2019;205(7):891–904. doi:10.1080/00295450.2018.1551988.
[43] Abedin KM, Haider AFMY, Rony MA, Khan ZH. Identification of Multiple Rare Earths and Associated Elements in Raw Monazite Sands by Laser-Induced Breakdown Spectroscopy. Opt. Laser Technol. 2011;43(1):45–9. doi:10.1016/j.optlastec.2010.05.003.
[44] Alamelu D, Sarkar A, Aggarwal SK. Laser-Induced Breakdown Spectroscopy for Simultaneous Determination of Sm, Eu and Gd in Aqueous Solution. Talanta 2008;77(1):256–61. doi:10.1016/j.talanta.2008.06.021.
[45] Jung EC, Lee DH, Yun J-I, Kim JG, Yeon JW, Song K. Quantitative Determination of Uranium and Europium in Glass Matrix by Laser-Induced Breakdown Spectroscopy. Spectrochim. Acta Part B At. Spectrosc. 2011;66(9–10):761–4. doi:10.1016/j.sab.2011.09.002.
[46] Hotokezaka H, Tanaka S, Suzuki A, Nagasaki S. Speciation Analysis on Europium(III) Using Laser-Induced Breakdown Spectroscopy. Radiochim. Acta 2000;88(9–11):645–50. doi:10.1524/ract.2000.88.9-11.645.
[47] Lawler JE, Sneden C, Cowan JJ, Ivans II, Den Hartog EA. IMPROVED LABORATORY TRANSITION PROBABILITIES FOR Ce II, APPLICATION TO THE CERIUM ABUNDANCES OF THE SUN AND FIVE *r*- PROCESS-RICH, METAL-POOR STARS, AND RARE EARTH LAB DATA SUMMARY. Astrophys. J. Suppl. Ser. 2009;182(1):51–79. doi:10.1088/0067-0049/182/1/51.
[48] Lawler JE, Hartog EAD, Sneden C, Cowan JJ. Sm Transition Probabilities and Abundances. arXiv October 19, 2005. http://arxiv.org/abs/astro-ph/0510585 (accessed 2022-05-18).
[49] Lawler JE, Wickliffe ME, Cowley CR, Sneden C. ATOMIC TRANSITION PROBABILITIES IN Tb II WITH APPLICATIONS TO SOLAR AND STELLAR SPECTRA. The Astrophysical Journal Supplement Series 2001;137:341–9.
[50] Den Hartog EA, Lawler JE, Sneden C, Cowan JJ. Improved Laboratory Transition Probabilities for Gd II and Application to the Gadolinium Abundances of the Sun and Three *r* -Process Rich, Metal-poor Stars. Astrophys. J. Suppl. Ser. 2006;167(2):292–314. doi:10.1086/508262.
[51] Rehse Steven J, Ryder Caleb A. Laser-Induced Breakdown Spectroscopy for Branching Ratio and Atomic Lifetime Measurements in Singly-Ionized Neodymium and Gallium. Spectrochim. Acta Part B 2009;64:974–80.
[52] Campbell KR, Judge EJ, Barefield JE, Colgan JP, Kilcrease DP, Czerwinski KR, Clegg SM. Laser-Induced Breakdown Spectroscopy of Light Water Reactor Simulated Used Nuclear Fuel: Main Oxide Phase. Spectrochim. Acta Part B At. Spectrosc. 2017;133:26–33. doi:10.1016/j.sab.2017.04.006.